Surface & Coatings Technology 465 (2023) 129585

Contents lists available at ScienceDirect

Surface & Coatings Technology

journal homepage: www.elsevier.com/locate/surfcoat

Setting a comprehensive strategy to face the runback icing phenomena

Julio Mora [a,*], Paloma García [a], Francisco Carreño [a], Miguel González [a], Marcos Gutiérrez [a], Laura Montes [b], Victor Rico Gavira [b], Carmen López-Santos [b,c], Adrián Vicente [d,e], Pedro Rivero [d,e], Rafael Rodríguez [d,e], Silvia Larumbe [f], Carolina Acosta [g], Pablo Ibáñez-Ibáñez [h], Alessandro Corozzi [i], Mariarosa Raimondo [i], Rafal Kozera [j], Bartlomiej Przybyszewski [k], Agustín R. González-Elipe [b], Ana Borrás [b], Francisco Redondo [l], Alina Agüero [a]

[a] Instituto Nacional de Técnica Aeroespacial, Área de Materiales Metálicos, Ctra. Ajalvir Km 4, 28850 Torrejón de Ardoz, Spain
[b] Nanotechnology on Surfaces and Plasma, Institute of Materials Science of Seville (CSIC-US), Americo Vespucio 49, 41092 Seville, Spain
[c] Departamento de Física Aplicada I, Escuela Politécnica Superior, Universidad de Sevilla, c/ Virgen de Africa s/n, 41011 Seville, Spain
[d] UPNA—Department of Engineering, Public University of Navarre, Campus Arrosadía s/n, 31006 Pamplona, Spain
[e] INAMAT2 – Institute for advanced Materials and Mathematics, Public University of Navarre, Campus Arrosadía s/n, 31006 Pamplona, Spain
[f] AIN—Centre of Advanced Surface Engineering, 31191 Cordovilla, Spain
[g] AIMPLAS—Instituto Tecnológico del Plástico, València Parc Tecnològic., Calle Gustave Eiffel 4., 46980 Paterna, Valencia, Spain
[h] Laboratory of Surface and Interface Physics, Department of Applied Physics, University of Granada, Campus de Fuentenueva, Es-18071 Granada, Spain
[i] Institute of Science, Technology, and Sustainability for Ceramics, CNR-ISSMC, Via Granarolo 64, Faenza, RA 48018, Italy
[j] Technology Partners Foundation, 5A Pawinskiego Str., 02-106 Warsaw, Poland
[k] Faculty of Materials Science and Engineering, Warsaw University of Technology, 141 Woloska Str., 02-507 Warsaw, Poland
[l] Airbus Defence & Space, Military Aircraft Engineering, TEYP, Avda. John Lennon s/n, 28906 Getafe, Spain

ARTICLE INFO

Keywords:
Aeronautic icing
Anti-icing material
Wetting
Surface
Runback icing

ABSTRACT

The development of anti-icing robust surfaces is a hot topic nowadays and particularly crucial in the aeronautics or wind energy sectors as ice accretion can compromise safety and power generation efficiency. However, the current performance of most anti-icing strategies has been proven insufficient for such demanding applications, particularly in large unprotected zones, which located downstream from thermally protected areas, may undergo secondary icing. Herein, a new testing methodology is proposed to evaluate accretion mechanisms and secondary icing phenomena through, respectively, direct impact and running-wet processes and systematically applied to anti-icing materials including commercial solutions and the latest trends in the state-of-the-art. Five categories of materials (hard, elastomeric, polymeric matrix, SLIPS and superhydrophobic) with up to fifteen formulations have been tested. This Round-Robin approach provides a deeper understanding of anti-icing mechanisms revealing the strengths and weaknesses of each material. The conclusion is that there is no single passive solution for anti-ice protection. Thus, to effectively protect a given real component, different tailored materials fitted for each particular zone of the system are required. For this selection, shape analysis of such a component and the impact characteristics of water droplets under real conditions are needed as schematically illustrated for aeronautic turbines.

1. Introduction

Atmospheric icing is a global issue that seriously affects many relevant industrial sectors, where the variety of icing mechanisms is as diverse as the targeted applications. One of the most critical sectors undergoing atmospheric icing is aeronautics, where ice accreted on different parts of the aircraft can severely affect aerodynamics, communications and a variety of sensors. To mitigate such issues, the most sensitive devices are equipped with ice protection systems (IPSs) either to avoid ice accretion (anti-icing) or to release the ice once it has formed (de-icing) [1]. Currently applied IPSs utilize external energy and are considered active systems. Most common active system technologies

* Corresponding author.
E-mail address: jmornog@inta.es (J. Mora).

https://doi.org/10.1016/j.surfcoat.2023.129585
Received 17 March 2023; Received in revised form 27 April 2023; Accepted 28 April 2023
Available online 8 May 2023

rely on mechanical [2], chemical [3] or thermal processes [4–6]. The latter is surely the most mature IPS currently applied in the aircraft industry [7].

However, such thermal procedures still suffer drawbacks that call for proper solutions. This is the case of the so-called runback icing, or secondary icing, a phenomenon that occurs downstream of thermally protected areas both in aircrafts and wind turbines. It is caused by melted ice originated in a non-fully evaporative de-icing operation, or from an IPS operated in running-wet or anti-icing modes [1]. By these secondary de-icing processes, the resulting liquid water flows and freezes on unprotected zones situated downstream of the heated zone.

During certain flight phases, runback icing represents a highly risky issue that may seriously disturb the aerodynamic conditions due to frozen rivulets. Several recent studies have dealt with this risk [8–10], for example, Whalen et al., studying the aerodynamic effects of this type of icing on an airfoil, found an increase of 80 % in the drag coefficient as compared with pristine surfaces or, in the worst case, a reduction of 50 % of the maximum lift coefficient [11].

Runback icing also takes place in other elements with geometries different from that of wings or aerodynamic airfoils. A typical case is that of the inside of engine air intakes [12,13] (see Fig. 1 Left). These components present zones where supercooled water droplets impinge during flight at a high angle of incidence, giving rise to two different icing processes based on different mechanisms: 1) icing by supercooled droplets impingement and 2) running-wet icing of water coming from the heated areas. Fig. 1 Right) schematically represents these two kinds of icing mechanisms.

Turbines have been proposed as a model system to study the application of passive solutions to avoid or minimize this type of icing processes through the modification of the surface characteristics. Different surface terminations have been reported in the literature, including materials with low wettability, hydrophobic or superhydrophobic [14], low surface energy materials [15], slippery liquid infused porous surfaces (SLIPS) [16], elastomers [17] and hard low roughness materials. Herein, we will test candidates representative of this ample selection of materials to get a systematic analysis of their response under well-defined icing conditions in a unique experimental set-up. This approach will avoid possible discrepancies due to differences in the experimental conditions, as it may happen when comparing literature data from various laboratories and testing methodologies. A summary of relevant properties regarding the potential anti-icing functionality of coatings or bulk materials within these categories is included in the materials and methods section.

In this study, a new dedicated testing methodology has been developed to separately simulate the different icing phenomena that take place on the model air intake device (Fig. 1): direct impingement of supercooled droplets and running-wet icing mechanisms. This methodology has been used to test materials within the aforementioned anti-icing categories, which also include commercial references representing the current state of the art of anti-icing strategies. Surface characterization methods to determine wetting properties, roughness, and ice adhesion have been also applied to screen the coating's behaviour, deduce their different anti-icing effects and ultimately select the most effective surface terminations to prevent icing. The main expected contribution of this kind of Round-Robin analysis is not limited to finding suitable candidates for current applications but also learning about the anti-icing phenomenology of these materials to determine their suitability for real specific zones of the air inlet of a turbine. This working methodology could pave the way to extrapolate their use to other fields of applications, where different passive strategies could work in different areas attending to their specific icing mechanism.

2. Materials and methods

2.1. Materials

Various types of bulk materials and coatings have been selected for this comparative study. They encompass five different categories with basic characteristics regarding their surface termination and interaction capacity with water/ice that are briefly described below:

a) Materials with low wettability: superhydrophobic materials (SHP):
The selection of this type of material relies on the assumption that a low liquid water/surface interaction also entails a reduced ice/surface interaction [18,19]. Thus, surfaces with water contact angles (WCA) between 90° and 150°, typical of hydrophobic materials (HP), or higher than 150°, considered as super-hydrophobic (SHP), are good candidates to exhibit anti-icing behaviour. Since the maximum WCA achievable as a mere result of chemical composition is close to 110° (e.g. for flat and smooth Teflon surfaces) SHP surfaces must have as an additional requirement a very high roughness, both at micro- and/or nano-scales. Particularly interesting in this regard are the Cassie-Baxter SHP surfaces depicting an anti-icing response based on reducing the water/surface effective contact area due to air pockets trapped in the micro-nanostructures of this type of hierarchical surfaces [20]. An example of this are the laser patterned structures which have been tested for anti-icing purposes [21,22]. It must however be stressed, that a high contact angle does not always imply a high anti-icing capacity [23–25]. As gathered in Table 1 four different super hydrophobic systems are analyzed in this article, including a commercially available reference.

b) *Polymeric matrix materials (PMM):* A reduced electronic interaction can minimize water or ice interaction with a surface, even though a high hydrophobicity is not achieved. The most representative

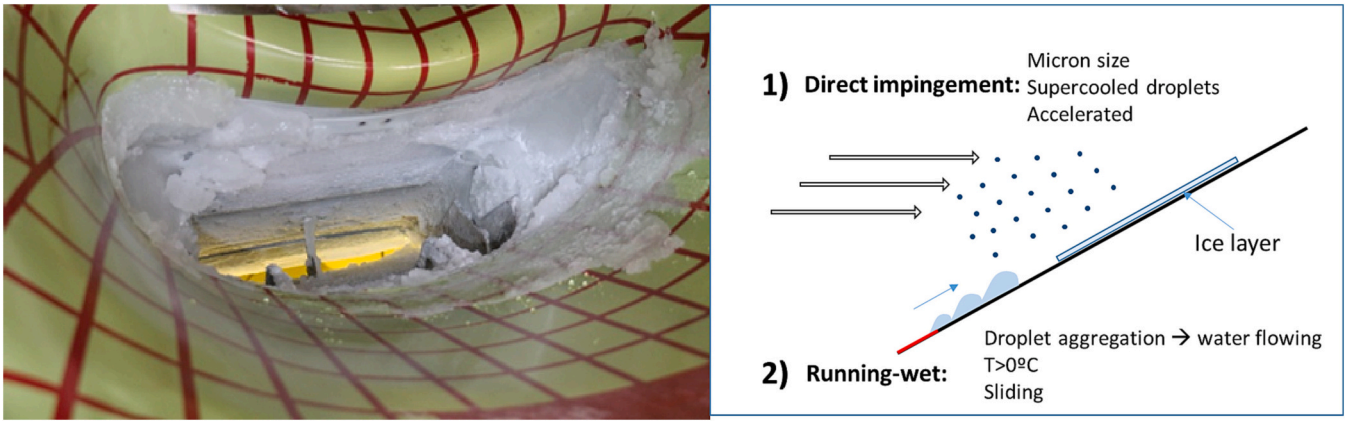

Fig. 1. Overview of The runback-ice issue. Left: Image of icing downstream from a heated area in an engine air inlet (courtesy from Airbus DS). Right: Scheme of icing mechanisms including ice accretion due to impingement of supercooled droplets and droplet aggregation flowing towards cooler areas and downstream icing.

Table 1
Lists the specific coatings and bulk materials tested in this study grouped according to the previous categories and provides additional information about each of them. A specific label has been assigned to each material/coating to ease their identification in the text. The commercial references denominations are followed by an asterisk:

Anti-icing strategy	Design characteristics	Proposed candidates	Denomination
Low roughness hard materials (HARD)	- Low surface roughness - High hardness, expected high durability	AA 6061-T6 (bulk) Anti-stick Quasicrystal coating (coating)	**HARD_1*** **HARD_2**
Polymeric matrix materials (PMM)	- Low surface roughness - Low surface energy	Polytetrafluoroethylene (PTFE) (bulk) Aerodur Aeronautic Polyurethane paint (coating) Siloxane modified Polyurethane paint (coating) Siloxane modified Polyester paint (coating)	**PMM_1*** **PMM_2*** **PMM_3** **PMM_4**
Elastomeric coatings (ELAS)	- Low surface roughness - Low surface energy - Good water mobility - Low ice adhesion	NuSil by Avantor (coating) Silicone oil-infused PDMS (coating)	**ELAS_1*** **ELAS_2**
Slippery liquid infused porous surfaces (SLIPS)	- Medium-high surface roughness - Low surface energy - Good water mobility - Low ice adhesion	PVDF-HFP electrospinning matrix + silicone oil (coating) Al_2O_3 matrix + perfluoropolyether (PFPE) lubricant oil (coating) SiO_2 matrix + perfluoropolyether (PFPE) lubricant oil (coating)	**SLIPS_1** **SLIPS_2** **SLIPS_3**
Superhydrophobic (SHP)	- High hierachical surface roughness - Low surface energy - Excelent water mobility	NeverWet by Rust-Oleum (coating) Organosilane-type modified Polyurethane paint (coating) Laser treated AA6061 + Al_2O_3 + PTOTES (Surface Treatment) Laser treated AA6061 + STA treatment (Surface Treatment)	**SHP_1*** **SHP_2** **SHP_3** **SHP_4**

materials in this category are some fluorinated polymers [26,27], which have shown promising performance but low durability. Silicones [28] and modified polyurethane coatings [29] have also reported anti-icing performance.

c) Slippery liquid infused porous surfaces (SLIPS):
In this case, a lubricant fluid is infused in a porous or textured surface to minimize the ice/surface interaction. Since 2011, when this type of material was first introduced [30], many studies have reported low ice adhesion values [31–33], with some of these surface terminations presenting the lowest ice adhesion values ever reported for this category [34,35]. These materials are usually characterized as HP with moderate WCA (90–110°), but very low sliding angle (SA) and contact angle hysteresis (CAH) values and excellent water mobility. Their main drawback, however, is the depletion of lubricant content upon operation, meaning that it must be reapplied after several usages.

d) Elastomeric coatings (ELAS):
These polymeric elastic surfaces have low elastic moduli and high deformability properties, which can lead to quite low ice adhesion [36,37]. By increasing the roughness and/or creating structures in elastomeric surfaces, both SHP and low ice adhesion can be achieved [38]. Moreover, elastomeric matrix SLIPs have been produced using polymeric porous scaffolds infused with lubricants [39].

e) Low Surface Energy and hard material (HARD):
Although a clear concept of low interacting material and its relation with anti-icing behaviour is not yet available, anti-stick quasicrystal (QC) materials can be also considered within this category. These have a cluster microstructure that generates reduced electronic density and low surface energy [40,41]. In previous work, some QC materials have shown low ice accretion [42] as well as low ice adhesion and interfacial toughness [43], while hardness was 4 times higher than that of the reference AA6061-T6, which has been proposed as aeronautic commercial reference of hard material with no anti-icing performance.

The anti-icing coatings/surface treatments and commercial references were applied on AA6061-T6 coupons (100 × 50 × 3 mm and 50 × 50 × 3 mm sizes). The application process, the provider, and related references for comparative analysis are included as Supplementary material (Section S1).

2.2. Surface characterization: roughness and wetting

Surface roughness was measured using a confocal microscope (model S-mart, SENSOFAR METROLOGY, Barcelona, Spain). The confocal microscope applies a Corse Shift single algorithm with an EPI 20× V35 lens for an area of 850.05 × 709.32 μm^2. According to the standard ISO 4287, the roughness profiles (S-L) measurements have been retrieved with three different filters: a low filter (F-operator-level, plane), a high filter (S-filter, standard cut off λs: 2.5 μm), and a Gaussian filter (L-filter, standard cut off λc: 0.25 mm). An average value was obtained from measurements taken at five different locations.

For non-static processes like ice detaching, besides the static wetting contact angle (WCA), dynamic wetting properties are also relevant. Therefore, characteristic features such as the sliding angle (SA), defined as the minimum inclination angle for a droplet to slide over the surface, or the contact angle hysteresis (CAH), which accounts for the maximum deformation of the droplet before sliding following the inflating/deflating method, have been also determined. The wetting properties were determined using an Optical tensiometer (Biolin scientific Theta lite) from Lasing, S.A. Madrid (Spain). The mean values were obtained from three measurements using 5 μL of deionized water for the static WCA, and 10 μL for the dynamic properties: SA and CAH.

2.3. Ice testing

2.3.1. Icing wind tunnel (IWT) and icing experiments

One of the main characteristic features of aeronautic icing is ice accretion by high-velocity impingement of supercooled droplets, a process that can be reproduced in an Icing Wind Tunnel (IWT). In this work, INTA's lab scale IWT (Fig. 2a) was used to simulate realistic ice accretion processes.

2.3.2. Ice adhesion by centrifuge test

Ice adhesion was evaluated according to the centrifuge methodology [44], following the procedures previously reported [45] (Fig. 2b-ii). The mean value of ice adhesion stress (KPa) from three tests for every sample was taken as representative of this parameter. Before ice adhesion evaluation, homogeneous glaze ice layers were accreted on the 50 × 50 mm samples, covering one-half of one side on every sample (12.5 cm^2) (Fig. 2b-i). The icing conditions were: Air Velocity: 70 m/s, Total Air

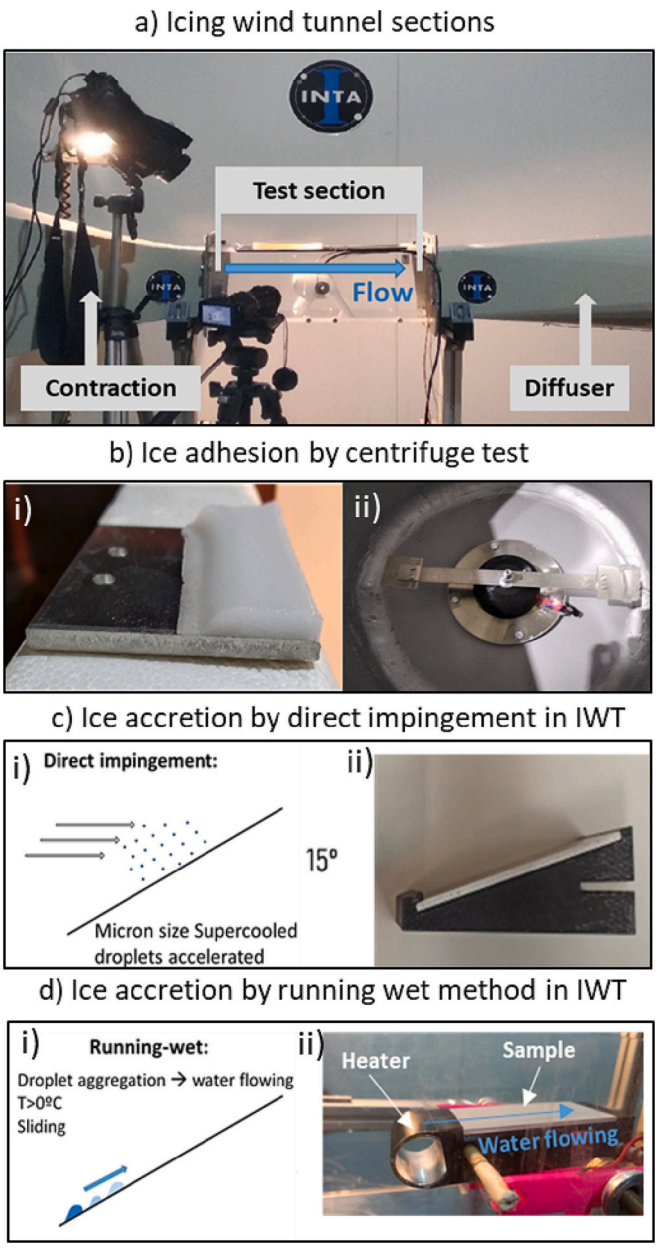

Fig. 2. Testing descriptions. (a) Image of Icing Wind Tunnel sections [45]; (b) Ice adhesion test: i) Detail of ice accreted on a sample; ii) Centrifuge system; (c) Direct impingement test: i) Mechanism scheme; ii) Specimen in the holder; (c) Running-wet test: i) Mechanism scheme; ii) Testing system includes a heater to simulate the running-wet process.

Temperature (TAT): −5 °C, Liquid Water Content (LWC): 1 g/m^3 and Median Volume Diameter (MVD): 20 μm.

2.3.3. Ice accretion by direct impingement tests in IWT

As described in the introduction, in those zones of the model air inlet system subjected to direct impingement of droplets coming from the airflow, ice accretion caused by supercooled droplets can be quite significant. To study this accretion process, a dedicated sample holder was designed where samples are placed at an incidence angle of 15° (Fig. 2c-i/ii).

The icing conditions were: Air Velocity: 35 m/s, TAT: -15 °C, LWC: 1.0 g/m^3 and MVD: 20 μm, to obtain glaze ice. After 2 min under these conditions, the surface of the samples was analyzed to qualitatively evaluate the covered area and amount and type of ice accreted. All tests were video recorded.

Python and the package "open-cv" have been used for image processing. The main goal of this processing was to have a numeric estimation of the percentage of ice-covered areas to perform a semi-quantitative comparison between samples. For the processing of the images, only the pixels inside a predefined rectangle were selected. The area was large enough to be representative of the zone of samples accreted with ice. To consider a pixel inside the image as ice, its aspect was compared with a colour threshold (on red, green and blue channels independently) previously defined for each sample depending on surface colour, reflectivity, or the incident light onto its surface. The pixels that were considered as ice were counted and compared with the total number of pixels that are inside the examined rectangle, thus obtaining the percentage of surface covered with ice. An additional factor for consideration in the analysis of the percentage of area covered by ice is the effect of perspective (angle used to take the photographs) on the software evaluation of the pixels. This may produce small inaccuracies in the relationship between the pixel size and its equivalent length and therefore in the final percentage of ice-covered area. An example of the way how the software deals with real photographs are reported in Supplementary Information S2 (Fig. S2). Taking this source of inaccuracy into account, the area percentage covered by ice is handled in a semiquantitative way in this work.

2.3.4. Ice accretion by running-wet tests in IWT

In the running-wet icing process, water flows from an upstream heated area of the sample. In this case, the designed holder places the sample at −5° of incidence angle relative to the airflow direction and includes an upstream heated zone emulating the action of a thermal IPS placed in the leading edge section when operated in anti-icing mode (Fig. 2d-i/ii). The tests were performed according to the following procedure:

1. The sample + holder block was placed in the IWT at TAT: −5 °C.
2. The air velocity was set at 35 m/s.
3. Then the heater was set to reach a stable 0 to 5 °C surface temperature (anti-icing mode).
4. A nebulization cloud was applied during 2 min of exposure (LWC: 1.0 g/m^3 and MVD: 20 μm).

In these conditions, the supercooled water cannot freeze in the heated leading edge section and flows through the test specimen until it freezes (runback freezing). After 2 min, the samples were analyzed and compared to evaluate the amount and type of ice accreted, as well as the percentage of covered area. All the tests were video and thermographically recorded.

The most promising candidates from the 2 min running-wet screening tests were subjected to longer cycles (15 min) following the same methodology until an eventual loss of performance and/or a relevant ice accretion takes place.

3. Results and discussion

3.1. Roughness and wetting behaviour

The roughness measurements and the wettability parameters of all samples are gathered in Table 2.

Data in Table 2 reveal significant differences among materials of different categories and, within the same category, also from one surface termination to another. These differences will be used to account for or, at least partially explain, the different data derived from the icing-test results in Section 3.2. As a summary, Fig. 3 shows a schematic view of the static and dynamic wettability behaviours found for the investigated materials as a function of the sample characteristics such as roughness and drop mobility.

According to this schematic representation, materials of the HARD category have a smooth finishing (especially in polished QC) and, in

Table 2
Roughness and wetting characterization at room temperature.

Material	Roughness (Sa - μm)	Std. Dev	WCA (°)	Std. Dev	CAH (°)	Std. Dev	SA (°)	Std. Dev
HARD_1	0,22	0,11	90	1,4	90	–	60	–
HARD_2	0,08	0,01	96,9	5	96,9	–	60	–
PMM_1	0,14	0,03	101	3	20	2,6	20	3
PMM_2	0,08	0,01	72,7	4,9	72,7	–	60	–
PMM_3	0,83	0,23	90	1,5	20,3	3,5	60	–
PMM_4	0,05	0,03	74	0,3	74	–	60	–
ELAS_1	0,06	0,01	115,1	1,7	30,2	4,5	60	–
ELAS_2	0,02	0,00	103,8	3,7	0	0	25	0
SLIP_1	1,19	0,64	155,8	0,3	16	2	14	2
SLIP_2	0,93	0,53	120	2,1	3	0,8	2	0
SLIP_3	0,37	0,05	121	1,9	6	2	12	3
SHP_1	2,78	0,50	166	0,5	6	1	5	1
SHP_2	0,95	0,18	148,9	1,2	148,9	–	60	–
SHP_3	39,15	7,10	175	0,5	6	0,6	4	1
SHP_4	13,71	2,40	170	0,8	6	0,8	4	1

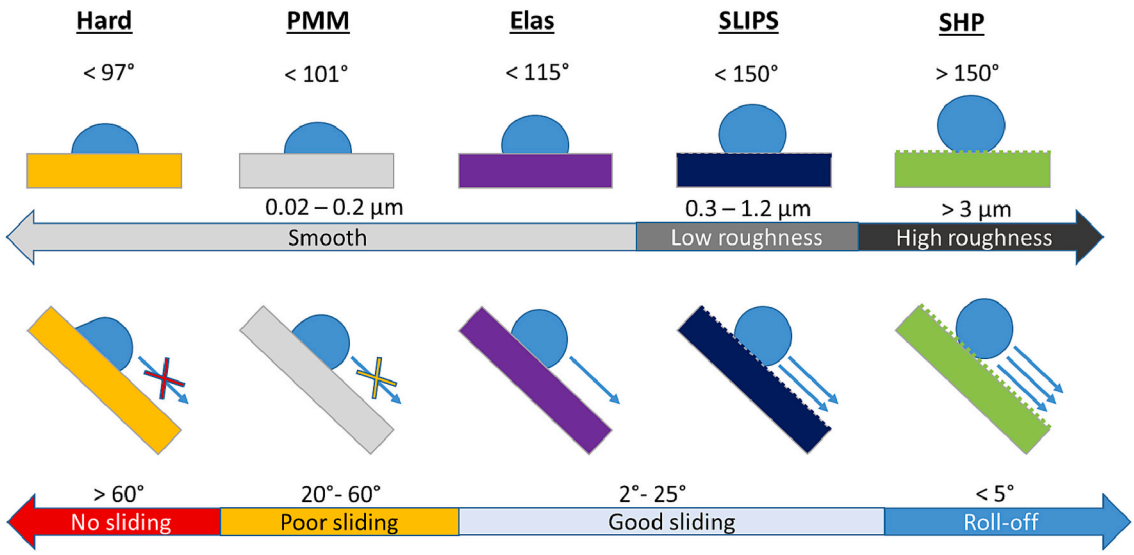

Fig. 3. (Top) Schematic representation of static WCA and roughness levels. (Bottom) Schematic representation of water mobility.

general, their surfaces show a strong interaction with water that prevents easy sliding despite droplet deformation. The PMM materials (except PMM_3) have smooth surfaces and present a relatively weak interaction with water that contribute to a decrease of the droplet deformation (lower CAH) but at the expense of poor drop mobility. ELAS are very smooth and present hydrophobic behaviour due to the low surface energy of silicone. The high water mobility reached on the surface of ELAS_2 is however noteworthy. A clear indication of their high sliding capacity has been drawn during the inflating/deflating test where a null contact angle hysteresis has been measured. The porous surface of the scaffold developed for the SLIPS coatings makes them sufficiently rough to display a high static WCA. SLIPS_1 reaches even superhydrophobicity, while SLIPS_2 and SLIPS_3 are hydrophobic with WCA ~120°. The low CAH and SA are indicative of excellent water mobility. The water/surface interaction in SHP materials is the weakest of all tested materials. Finally, the wetting behaviour of SHP coatings, except for SHP_2, can be described by a Cassie-Baxter state model with very low roll-off angles. The high WCA (especially in the two laser-treated metallic alloys, samples SPH_3 and SHP_4) depends on the roughness induced on the surface and the resulting relatively low contact area with a water drop on top.

3.2. Ice testing behaviour

3.2.1. Ice adhesion stress

Several ice adhesion testing methodologies based on various detachment principles under different icing conditions can be found in the literature [46]. In this way, the icing procedure is one of the most relevant differential factors when comparing ice adhesion results from different research groups. Ice can be formed in molds inside a freezer, or by the impingement of supercooled microdroplets that freeze immediately when they impact the surface. Ice formed by impact is closer to the real conditions found in an icing cloud and similar to the airflow inlet model system selected for testing in this work.

Ice detachment by centrifuge forces is a widely spread methodology that keeps the ice unaffected during the tests, avoiding push or pull stresses caused by external testing elements.

The ice adhesion results obtained for the tested materials are shown in Fig. 4.

It is noteworthy regarding data in Fig. 4 that the reported average values are the result of a relatively large dispersion of data. Such dispersion is common in this type of adhesion test where different adhesion values can be obtained for various repetitions with the same sample and ice accretion methodology. However, data in Fig. 4 depicts clear trends enabling the establishment of the following ranking for the ice-adhesion performance (better performance corresponds to lower adhesion, the list also includes two spplited materials, PTFE and AA

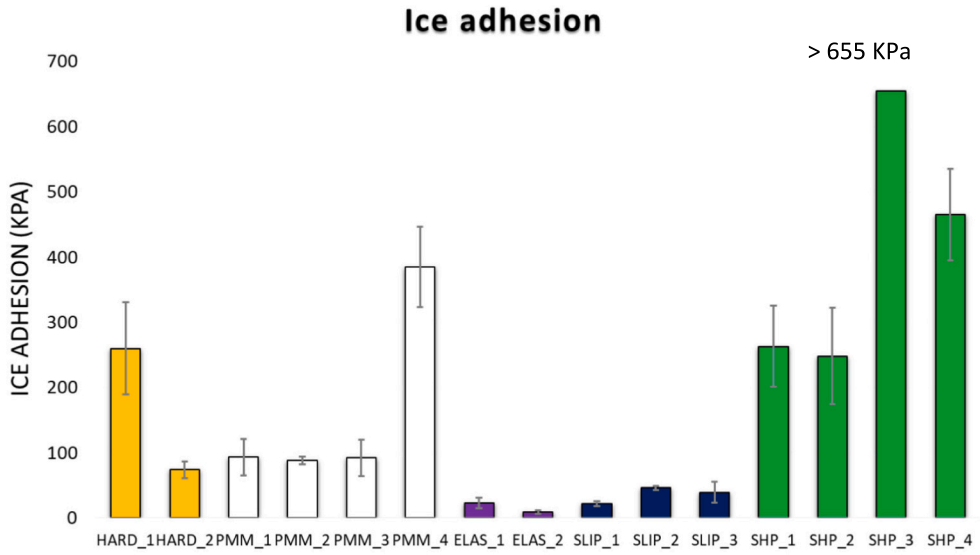

Fig. 4. Ice adhesion stresses of the different tested samples colour-grouped by categories of materials. Please note that there is no error bar in SHP_3 because the centrifuge reached its maximum rotation velocity without shedding the ice. The adhesion value, in this case, is, therefore, higher than 655 KPa.

6061-T6 commonly used as references): ELAS > SLIPS > HARD_2 > PTFE > PMM > AA 6061-T6 > SHP.

As previously reported, elastomers and SLIPS samples showed low adhesion values [33,47], feature that can be attributed to the incorporation of a liquid lubricant on the SLIPS surfaces in direct contact with the ice. This produces a decrease in the effective ice contact area, minimizing the nucleation sites and, consequently, the adhesion of ice layers [48]. The tested SLIPS had adhesion values in the range of 22–46 KPa, and the best result (22 KPa) was obtained for SLIP_1 consisting of a fluorinated polymer matrix infused with silicone oil. Ice adhesion was almost twice (close to 40 KPa) in samples SLIP_2 and SLIP_3 consisting of a ceramic matrix infused with perfluorinated oils.

ELAS samples presented adhesion stresses in the remarkable range of 9–23 KPa, 3 to 9 times lower than PTFE (PMM_1), known as a low ice adhesion reference. These results are in good agreement with reported works, where these materials exhibited some of the lowest values so far known. For example, He et al. [49] reported a super-low ice adhesion surface (SLIAS) consisting of PDMS-based coatings and proposed a macroscale-initiator (MACI) mechanism in which the coating deformability plays an important role as a crack initiator in the ice-surface interaction. Similarly, Golovin et al. described a good ice adhesion performance for other icephobic elastomers, especially for pieces with large sections, where a low interfacial toughness seems to be beneficial for ice detachment [50].

From the PMM group of materials, the aeronautical polyurethane paint (PMM_2) showed fair behaviour, comparable to that of PTFE. A relatively low ice adhesion in aeronautic-certified polyurethane paints has been previously reported [51]. The PDMS-modified polyurethane paint (PMM_3), which achieved higher WCA but lower water mobility than the non-modified polyurethane, did not improve the adhesion behaviour, probably because of its higher roughness.

Although a poorer performance was found in general for the HARD materials (this was confirmed for sample HARD_1), an amazingly good result was obtained for the anti-stick QCs (HARD_2), characterized by a better performance than PTFE. Remarkably, the observed behaviour was even better than that obtained in previous Double lap shear and push testing experiments for in-mold-formed ice. As expected, bare AA6061-T6 (HARD_1) ice adhesion stress was high and similar to some previously reported values [44,52].

The highest values of ice adhesion stresses were obtained for SHP materials, likely due to the interlocking effect caused by the ice filling the hills/valleys levels of their surface roughness structure. Inside this group, two categories can be differentiated: SHP_1 and SHP_2 with roughness associated with a polymeric matrix and lower adhesion values, and SHP_3 and SHP_4 with multiscale roughness on metallic substrates and higher adhesion values.

In summary, 9 of 15 materials achieved ice adhesion values lower than 100 KPa, a magnitude that is deemed a threshold for low ice adhesion surfaces, and only one elastomeric material reached a value lower than 10 KPa, where detachment might be induced by natural forces, such as wind or gravity [53].

3.2.2. *Ice accretion by direct impingement in IWT*

The metastable state of supercooled water droplets can be easily altered by any kind of perturbation (e.g., an impact). On the other hand, the small size of cloud microdroplets causing icing in aeronautics minimizes the splashing effect, helps the ice nucleation and quickly leads to the formation of an ice layer strongly attached to the surface. There have not been passive solutions reported that completely avoid ice accretion, a process particularly critical onto perpendicular surfaces to the direction of incoming droplets.

In an engine air intake, as the one reported in Fig. 1 (Right), there are many different angles of incidence for the direct impingement of droplets. To consider this variability, for the current systematic study of materials, an angle of attack of 15° has been selected as representative of the wide range of angles encountered in a real situation.

Fig. S3 in the Supplementary Information shows images taken after icing, together with the calculated percentage of ice-covered area. The bottom section of each specimen is masked by the fixturing. Fig. 5 shows the summary of the percentages of ice-covered areas for the different materials. As deduced from this figure, a first assessment of the icing performance of the examined types of materials follows the order: ELAS ≥ SLIPS > SHP > HARD_2 > PMM > AA 6061-T6, from best to worst anti-icing behaviour.

A closer inspection of specific features in the images in Fig. S3 in the Supplementary Information and data in Fig. 5 provides interesting additional information. Thus, HARD_1 surface appears completely covered by ice, including some regions in the centre, where the formed ice was transparent. As for the ice adhesion results, ELAS and SLIPS samples prevent ice accretion. We think that the high water mobility on these materials evidenced by their low SA and CAH values (c.f. Table 2) is an important factor contributing to avoiding ice pinning and therefore

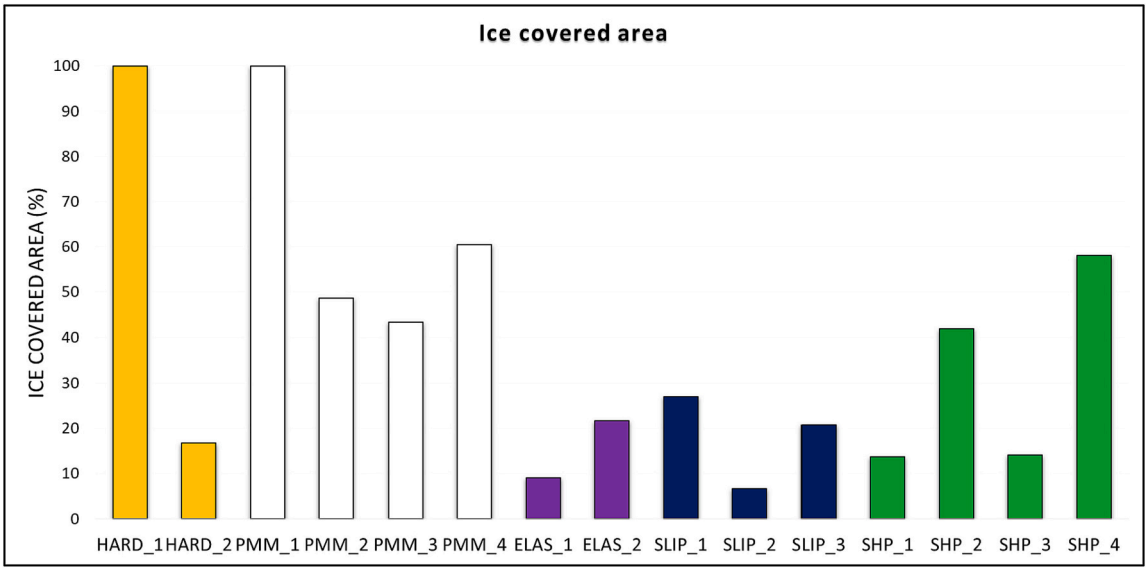

Fig. 5. Ice accretion by direct impingement in IWT. Comparison of the ice-covered area % in the different coatings.

to decreasing the icing rate. Very likely the low ice adhesion stress on these surfaces is an additional factor contributing to this functionality. This was supported by the observation of small water/ice aggregates and ice blocks moving under the action of the flowing air pressure on surfaces of these materials covered with accreted ice (see also Movie S1 as Supplementary Information S4).

Current tests with the SHP_1 coating confirmed its known optimal performance to delay ice accretion under natural icing conditions in anemometers [54], or even unmanned aerial vehicles UAVs [55] It was also found that this commercially available coating decreases the ice buildup on rotor blades and partially mitigates thrust losses [56]. In turn, SHP_3 material produced a decrease in ice accretion by 29 % with respect to an untreated aluminium alloy aerodynamic profile, keeping its good sliding behaviour during the entire 2 min of the test period. However, SHP_2 and SHP_4 materials did not demonstrate sufficiently good performance in this IWT test. SHP_2 neither showed significant water mobility, while SHP_4 lost its anti-icing performance after a few seconds of nebulization (see Movie S2, reported as Supplementary Material S5). From the percentages of ice-covered area in Fig. 5b and the just commented evidence, two conditions must be fulfilled to achieve a significant reduction of ice accretion from supercooled microdroplets on SHP materials: a) a high water mobility enabling an easy sliding or bouncing out of droplets before their freezing; b) a stable and durable Cassie-Baxter state to maintain the previous condition.

According to Fig. 5, PMM materials depicted a poor performance regarding ice accretion with the formation of big, partially connected ice agglomerates or islands. The percentage of the covered area of samples was rather high for all samples, particularly for sample PMMM_1. The uncoated HARD_1 aluminium alloy sample also depicted poor behaviour against icing, showing the worst performance of the whole series of investigated samples. In this sample, ice is accreted in the form of a continuous layer (i.e. 100 % coverage of surface area). Unlike this HARD_1 sample, the behaviour of sample HARD_2 (QC) was rather promising for harsh conditions applications (accreted percentages around 15 % according to Fig. 5b), particularly because it is a very hard material with a Vickers hardness of 5.1 GPa. The low accretion found in this test supports previous results with flat samples of this material for 90° of incidence angle, where a reduction of 28 % in ice accretion was found in comparison with uncoated AA6061-T6 [42]. The lower roughness of HARD_2 samples in the current experiment (Ra 0.08 Vs 0.20) and the different angles of incidence of impinging droplets (15°, vs 90°) account for the lower ice accretion found here.

Besides the percentage of surface area covered by ice (Fig. 5b), the assessment of the shape of ice aggregates is also a relevant differential characteristic of the icing behaviour. Particular shapes are tightly related to the degree of surface-water/ice interaction and, eventually, with the icing mechanisms. Detailed views of the accreted ice and proposed mechanisms responsible for the shape of the ice aggregates are reported in Fig. S6 in the Supplementary Information. The mechanism by which the incoming droplets become partially or totally detached from the materials after their impact determines the morphology of ice aggregates and how ice becomes accreted on the surface. High substrate-ice interaction and a low water release capacity of surfaces lead to the formation of continuous layers of ice (e.g., this happened on sample HARD_1). ELAS and SLIPS samples, characterized by moderate WCA values but favorable sliding, give rise to the formation of large contact area ice islands with low adhesion. In contrast, the SHP materials (characterized by a Cassie-Baxter wetting state) are characterized by both a high WCA and a high rolling capacity. As a result, these samples accrete ice aggregates with spherical/droplet-like shapes and small contact areas with the substrate, but high adhesion strengths.

3.2.3. *Ice accretion by running-wet in IWT*

The methodology implemented for this test permits the discrimination of the direct impingement of water droplets from a running-wet mechanism, enabling the separate evaluation of the latter. Running-wet tests were first done on sample HARD_1 with the leading edge heater OFF. As expected, an angle of incidence of −5° was too small to enable ice accretion on the impingement area of the leading edge, but it was enough for freezing on the "run back" section.

During the heating tests, the temperature of the leading edge section was close to 5 °C, high enough to inhibit ice accretion in this zone but low enough to avoid excessive heating of the downstream flowing water. Fig. S7 in the Supplementary Information shows photographs of the icing events taking place in running-wet mode on the different types of investigated materials.

In runback icing tests, the impinging water is slightly "heated" at the leading edge and slides on the surface in liquid form to reach the runback section. As a consequence, water mobility plays an important role. It is important to note that the incoming microdroplets may aggregate in the form of bigger droplets, rivulets, or water films. The various icing mechanisms expected to occur in running wet icing processes are described in Fig. 6 depending on the water sliding capacity on the surfaces. Antonini et al. described the mechanisms and differences in

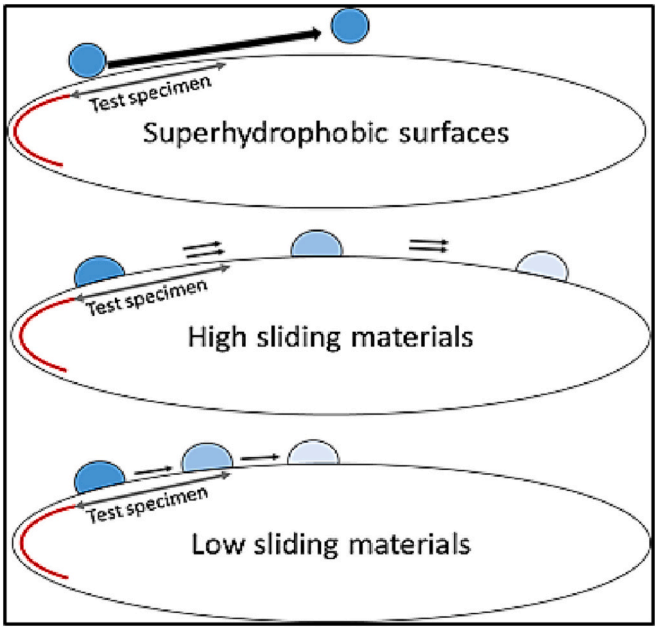

Fig. 6. Schemes of the different water roll-off/slide action mechanisms involved in the running-wet testing mode.

runback icing behaviour for hydrophilic and SHP surfaces [57]. According to this author, sliding droplets moving onto hydrophilic surfaces sooner or later freeze on the surface, while SHP surfaces reject (by rebounds or by roll-off) this water out of the surface, avoiding the accretion of ice.

In general, there was a good anti-icing performance for the different materials in the running-wet mode, although a clear classification by category of materials was not straightforward for this test. A rough classification based on visual observation of the amount of accreted ice would be the following: SHP > HARD_2 = PTFE = SLIP_2 = ELAS_2 > PMM = ELAS_1 > SLIPS > AA 6061-T6 = PMM_2, starting with the best performing material (less accretion, the list includes also the references PTFE and AA 6061-T6). Three types of icing stages have been taken into consideration to establish this ranking: ice that grows from the edges towards the sample centre, isolated ice islands, or the combination of both (for additional information, see also Fig. S8 in the Supplementary Information). We must note that for this evaluation, the ice accreted on the sample edges has been disregarded because accumulation in these zones may depend on small misalignments between the sample and holder (upper and lower edges) or defects generated during the sample cutting process (left and right edges).

It is noteworthy that, as revealed from the images in Fig. S7 in the Supplementary Information, the worst performance was found for materials that are currently used for aeronautical applications (HARD_1: AA6061-T6 and PMM_2: PU aeronautical paint), which stresses the need for new and reliable anti-icing materials or coatings. These materials presented two types of icing which were observable during the first seconds of nebulization. Remarkably, SHP materials kept their surface free of ice after 2 min of exposure, with just a few small ice islands formed on sample SHP_2 (this sample presented the lowest water mobility from all tested SHP materials).

Not only hydrophilic surfaces (WCA < 90°) promote a high surface-droplet interaction favouring freezing. Hydrophobic surfaces (90° < WCA < 150°) may also provide sufficient water-substrate contact area to ensure an effective heat exchange leading to freezing. Yet, other key factors of icing are the surface sliding capacity and the running-wet distance, the two of them affecting the contact time of droplets with the surface. Better sliding or shorter contact times reduce the interaction, and consequently the amount of accreted ice. Thus, the lower the sliding, the higher the interaction is, and the more ice forms.

The scheme in Fig. 6 represents the interaction mechanism on SHP surfaces and highlights why they are particularly well fitted for running wet anti-icing: the actual contact area is extremely low, there is no time for heat exchange and no effective nucleation sites can be found before the droplets are rejected by bouncing or rolling-off. Thus, once droplets take off from the surface and are beyond the influence of the aerodynamic boundary layer, they will not impact again on adjacent surfaces.

A second group of samples (HARD_2, ELAS_2, PMM_1, and SLIPS_2) depicted a low ice accretion at the edges, a behaviour that could be explained by a suitable combination of low surface energy, high sliding, and low roughness. SLIPS_1 and SLIPS_3, on the other hand, present a high level of icing at the specimens' edges, where ice begins to accrete already during the first few seconds of nebulization. In this case, the scattered and not-sticked ice deposits that form on the surface are likely attached to surface defects or are the result of limitations of the testing methodology.

Reliable anti-icing solutions must be durable and stable over time and prolonged use. Therefore, the most promising materials selected out of the 2 min screening running-wet tests were subjected to 15-min cycles following the same methodology, until ice accretion began to be observed. Photographs of the tested samples after 15 min of testing are shown in Fig. 7a.

This figure shows that SHPs materials presented the best performance, with icing occurring mainly at the edges of the samples. Significantly, other high sliding materials (HARD_2, ELAS_2, PMM_1, SLIPS_2) kept the anti-icing behaviour just for approximately 5 min, but after 15 min they accreted ice at the edges and in the form of islands on their central surfaces. The better performance of SHP materials was exemplified by an outstanding anti-icing resistance in sample SPH_3 where icing was completely neglected. To further test this anti-icing capacity, SHP_3 sample was subjected to three additional 15 min icing cycles to explore its limits and determine whether the performance may be lost. Images of this sample after each consecutive test are shown in Fig. 7b. Remarkably, the last 45 min icing cycle confirmed the exceptional behaviour of this coating material where no ice forms on the surface (ice only accretes at the upper side, where it is deposited on the heater wires and upper edge of samples). We link such outstanding performance to a permanent Cassie-Baxter state depicted by this sample all along the successive test cycles. It is also noteworthy that this sample did not present the rather common transition from a metastable Cassie-Baxter to a Wenzel state found upon exposure to high-humidity environments [58,59]. On contrary, sample SHP_3 held a stable Cassie-Baxter rolling-off capacity under the IWT icing in-cloud conditions, as well as in additional laboratory tests (see Movie S3 in Supplementary Information S9). It is also remarkable that these surfaces present durable freezing-delaying responses, with ice formation times from static drops to ice as long as 230 min at −5 °C [38].

4. Discussion

Since the testing methodology in this study has been developed to simulate specific conditions for a given application (i.e. engine air inlet), this discussion frames within these particular conditions only. For the first evaluation, we deemed it practical to rank the tested materials by their performance for five different functionalities. For this purpose, we assign numerical scores from 1 to 5, with 5 being the best performance and 1 the worst. Table 3 presents a relation of the assigned scores. The materials have been grouped in two sets, one formed by PMM_1, PMM_2 and HARD_2 materials and another set with the rest of the candidates. The materials in each group have been evaluated separately from those in the other.

Hardness and expected durability scores have been assigned considering the hardness and maintenance requirements expected for each type of material. In this regard, metals are the hardest, followed by

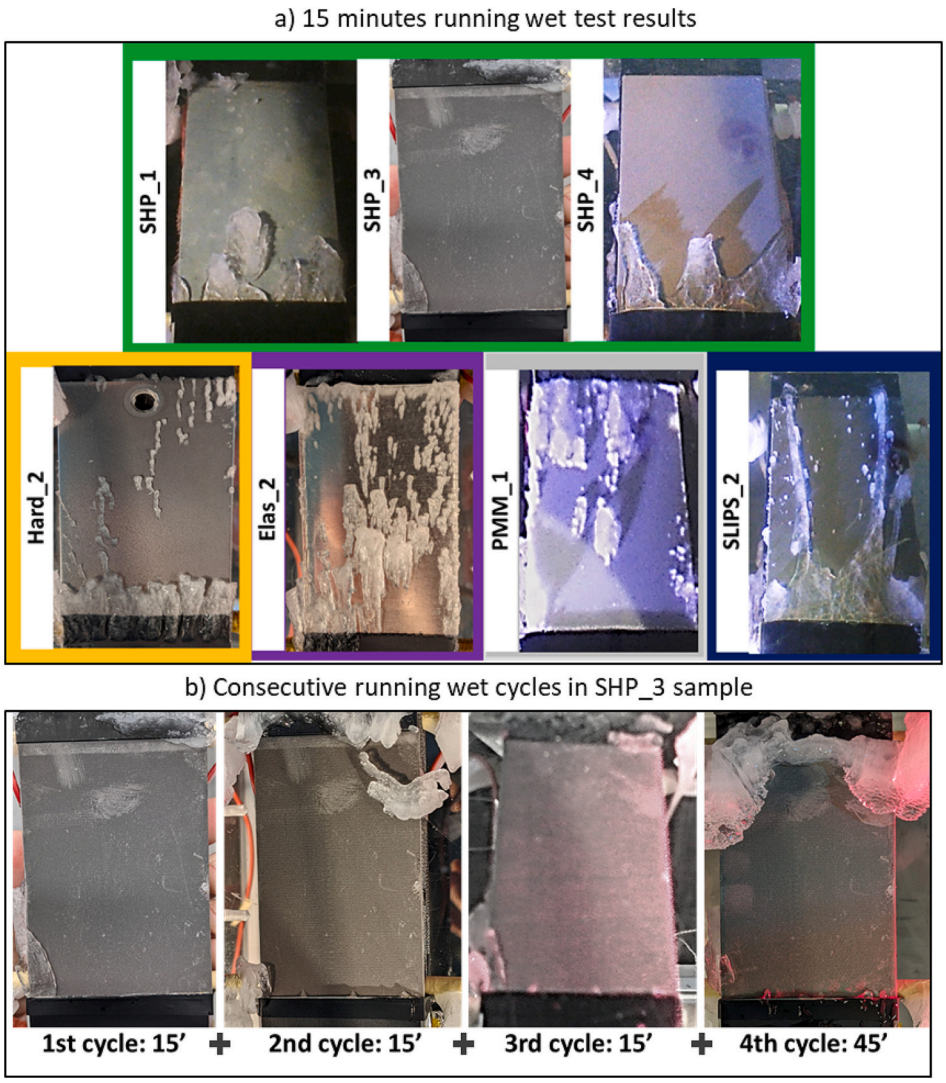

Fig. 7. Running wet experiments of long duration carried out for the different anti-icing surfaces. a) Images of selected materials after 15 min of running-wet testing; b) Images showing that sample SHP_3 kept the anti-icing performance after 3 successive icing cycles (15 min each) plus a subsequent 45 min icing cycle.

Table 3
Performance score for the tested materials.

Strategy/material	Low ice adhesion	Avoid icing by direct impingement at 15°	Avoid running wet icing at 5°	Water mobility	Hardness and expected durability
Hard_1 (AA 6061)	2	1	1	1	5
PMM	3	2	3	2	3
Elas	5	5	4	3	2
SLIPS	4	4	2	4	1
SHP	1	3	5	5	4
PMM_1 (PTFE)	3	1	5	3	3
PMM_2 (Aeronautic Paint)	3	2	1	2	3
Hard_2 (QC)	3	4	4	1	5

SHP laser-treated metallic alloys, then the polymeric materials, followed by the soft elastomers and finally SLIPS, as the latter requires replacing the lubricant periodically. This classification is only intended for the qualitative assessment of a functionality (durability), which is difficult if not impossible to evaluate quantitatively.

To better visualize the interplay of the assigned scores, they have been plotted in radar graphs to have a general picture of the capacities and limitations of the investigated materials. The results presented in Fig. 8a clearly illustrate the capacities and drawbacks of the materials under investigation in this study:

- HARD_1 (AA 6061-T6) and PMM_2 (Aeronautic paint): These commonly used aeronautic materials, despite their current and ample use in this field, showed poor behaviour in almost every category, highlighting the need for alternative anti-icing materials or coatings.

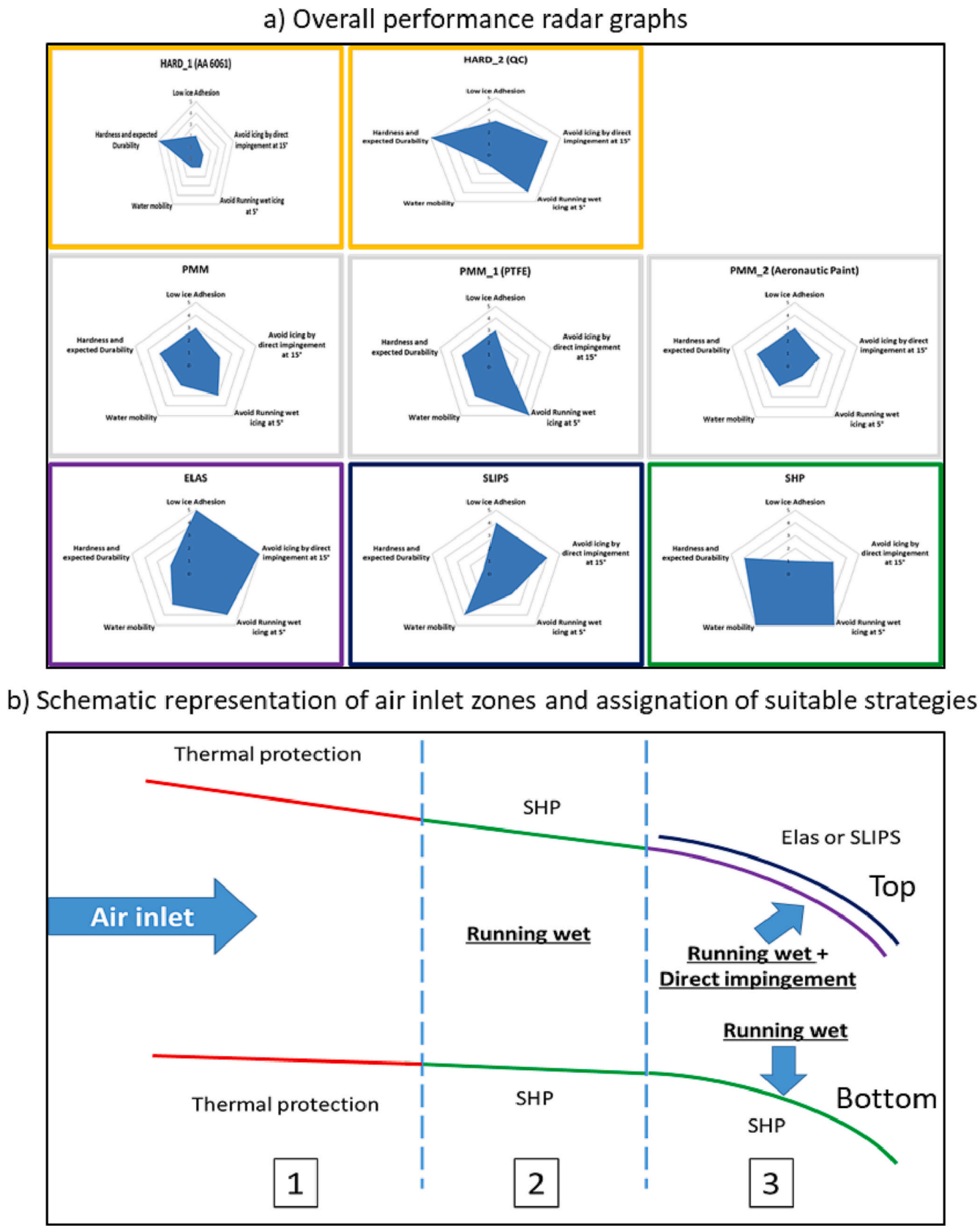

Fig. 8. Summary of the Round Robin-like approach. a) Radar graphs of assigned scares to the different samples for: Ice Adhesion, Icing prevention: Running-Wet and Direct Impingement, Droplet mobility and Durability; b) Schematic representation of an air inlet system (side view) divided into different sectors with reference to the expected icing mechanism in each zone and the proposed passive solution.

- HARD_2: The high hardness of this material, justifies a high erosion resistance and high durability. It also shows high scores regarding the delay of ice accretion under direct impingement and running-wet conditions. An ice adhesion lower than 100 KPa is already within the values considered low ice adhesion. In addition, this material has the longest expected durability and a reasonably good anti-icing performance.
- PMM: Although it is difficult to be categorical solely relying on the proposed score analysis, it appears that its anti-icing performance is better than that of currently used materials in aeronautics, but not good enough to represent a viable and durable alternative. A clear example of this limitation is PMM_1 (PTFE), which depicts a low ice adhesion and delays the running-wet icing, but has low hardness and strength, high wear rate, and therefore low durability [60]. Moreover, its performance under direct impingement of water droplets was simply unacceptable.
- ELAS: materials showed an outstandingly low ice adhesion, with very low adhesion stress values enabling ice detachment by natural forces (< 10 KPa). This property, combined with a high water sliding capacity, deals to excellent ice accretion delays in both direct impingement and running-wet modes. The main drawback is the expected low durability due to its low hardness. Conversely, its elastic resistance to impacts and high deformability have shown to be beneficial in abrasion and erosion tests, keeping an acceptable performance regarding ice adhesion, thickness loss and roughness modification [61].
- SLIPS: It behaves as ELAS, i.e., they are characterized by high water mobility, low ice adhesion, delay of ice accretion under direct impact and reasonably good running-wet performance. The need for frequent lubricant replacement is the major drawback of this promising strategy.
- SHP: The low water surface interaction of this material evidenced by the high WCA and outstanding roll-off capacity of its Cassie-Baxter state result in striking results in running-wet tests. Upon direct impact, the ice becomes accreted in droplets or aggregates with ball shapes and a small contact area with the substrate. However, the adhesion of these ice aggregates is extremely high due to the interlocking effects of ice distributed within the roughness features of the surface.

With this general evaluation analysis in mind, a general conclusion of the Round Robin-like analysis carried out in the present work is that no passive solution may completely and effectively protect against icing all zones of aeronautic devices under all possible atmospheric icing conditions. Since each material type has strengths and weaknesses, a combination of various materials, each one appropriate for each specific zone, might be the best approach for straightforward protection. Therefore, for any successful anti-icing strategy, it would be necessary to define differentiated zones or sectors where distinct icing mechanisms are expected. This analysis should take into account a wide range of experimental variables: air velocity, temperature, LWC, droplet size, angle of incidence, the influence of upstream zones, etc. A simplified approximation to this exercise for an engine air inlet entrance is schematically shown in Fig. 8b. Zone 1 in this scheme is thermally protected and therefore ice accretion does not occur in this zone. The resulting thawed flowing water will reach zone 2 pushed by the incoming air following a running-wet mechanism. The most suitable material to avoid accretion in this zone relies on SHP materials. The roll-off or bouncing water will finally reach zone 3, where different mechanisms in the top and bottom regions are expected. The lower region of zone 3 will have negative angles and an SHP material would be an optimal solution in the downstream part following zone 2. At the upper face of zone 3 a running-wet mechanism will be combined with a direct-impact icing mechanism due to the high incidence angles of water droplets impinging on this zone. Finding an anti-icing solution for this zone would be quite challenging because the ice will probably accrete no matter the material chosen. Therefore, instead of delaying icing, ELAS or SLIPS could surely be a good solution to promote ice detachment once it is formed due to the extremely low ice adhesion strengths found in these materials.

A deep known of the working modes of different anti-icing strategies will be a key factor to progress to reliable passive solutions or, at least, to improve the performance of hybrid systems [62–65].

5. Conclusions

A dedicated testing methodology to simulate icing mechanisms for a specific application (an engine air inlet) has been developed to evaluate different anti-icing passive strategies and materials: hard polished metallic materials (HARD), low surface energy polymeric matrix materials (PMM), Elastomers (ELAS), Slippery liquid infused porous surfaces (SLIPS) and superhydrophobic materials (SHP). Fifteen different materials including aeronautical and commercial references, as well as previously reported anti-icing materials, have been tested and systematically compared in a kind of Round-Robin analysis.

The overall conclusion of such a systematic work is that no unique passive solution may effectively protect all zones of the chosen device against ice formation. This limitation also applies to the different impacts expected for the large variety of possible atmospheric icing scenarios. From this analysis, some application conditions and limitations have been identified. The tested PMM material had a low ice adhesion (< 100 KPa) but did not behave well enough against ice accretion for both mechanisms, the direct impact of supercooled droplets and the running-wet conditions. ELAS achieved super-low ice adhesion (< 10 KPa) and got a good protecting performance against both mechanisms of ice accretion. With better water mobility than ELAS, SLIPS showed a slightly lower anti-icing performance, characterized by a quite low ice adhesion (22–39 KPa range) under the direct impact, but only a moderate or average testing behaviour in running-wet.

SHP materials were excellent in promoting water mobility on its surface, which resulted in an outstandingly good anti-icing running-wet performance, even after 45 min of anti-icing activity for the combination of laser treatment, nanocolumnar Al2O3 and perfluorinated grafting [22]. This promising candidate depicted a stable Cassie-Baxter state under the tested conditions. Direct impact icing was significantly reduced and gave rise to the formation of rounded ice aggregates with droplet shapes. However, an extremely high ice adhesion limits the use of this coating to completely hinder ice accretion. The major drawback of these materials is linked to their durability due to softness or maintenance requirements. In that direction, a tested polished quasicrystal material (5 times harder than aluminium alloy) could be an interesting durable candidate for anti-icing functionality. Its performance against icing was relatively good (i.e., it depicted a low ice adhesion and moderate ice accretion performance), while the expected durability was the best from all tested materials.

Ideally, tailored anti-icing methodologies should be developed to test the efficiency of advanced materials under specific conditions. The efficiency of each method should be demonstrated for each zone. We propose that despite the herein detected limitations of the tested passive anti-icing strategies, a combination of various materials chosen according to the areas of the devices to be protected can be a solution, even for a demanding application field such as aeronautics.

CRediT authorship contribution statement

The conceptualization of this work was carried out by J.M, P.G. and F·C.. The methodology and investigation was an iterative work of all the authors. M.G., L.M., V.R., C.L., A.V., S.L., C.A., P.I., A.C., B.P. provide the tested materials, which was tested by F·C and P.G.. M.G.dV. developed the used software. J.M was in charge of the original draft writing, while P.G., F.C., M.G.dV, A.B., A.R., A.C., A.A., J.M. worked in the writing-review and editing process.

Declaration of competing interest

The authors declare that they have no known competing financial interests or personal relationships that could have appeared to influence the work reported in this paper.

Data availability

Data will be made available on request.

Acknowledgement

The project leading to this article has received funding from the EU H2020 program under grant agreement 899352 (FETOPEN-01-2018-2019-2020 - SOUNDofICE). The authors also thank the MINECO-AEI (MAT2016-79866-R, PID2019-109603RA-I00 and PID2019-110430GB-C21) funded by MCIN/AEI/10.13039/501100011033 and by "ERDF (FEDER) A way of making Europe", to RTI2018-096262-B-C44–MAITAI, Multidisciplinary Approach for the Implementation of New Technologies to prevent Accretion of Ice on aircraft, funded by MCIN/AEI/10.13039/501100011033 (Ministerio de Ciencia, Innovación y Universidades—Retos) and CSIC 202160E002-217538, for financial support. CLS thanks the University of Seville through the VI "Plan Propio de Investigación y Transferencia de la US"(VI PPIT-US) and the Ramon y Cajal Grant program.

Appendix A. Supplementary data

The supplementary information section includes detailed experimental information on the preparation of anti-icing materials, and additional photographs and videos to complement the figures in the main text. Supplementary material associated with this article can be found, in the online version, at doi:https://doi.org/10.1016/j.surfcoat.2023.129585.

References

[1] FAA, Transportation, U. S. Department of. Aircraft Icing Handbook Vol. 2, 1991. Atlantic City.
[2] M. Endres, H. Sommerwerk, C. Mendig, M. Sinapius, P. Horst, Experimental study of two electro-mechanical de-icing systems applied on a wing section tested in an icing wind tunnel, CEAS Aeronaut. J. 8 (2017) 429–439, https://doi.org/10.1007/s13272-017-0249-0.
[3] Z. Goraj, An overview of the deicing and antiicing technologies with prospects for the future, in: 24th International Congress of the Aeronautical Sciences, Yokohama, Japan 29, 2004, pp. 1–11.
[4] M. Mohseni, A. Amirfazli, A novel electro-thermal anti-icing system for fiber-reinforced polymer composite airfoils, Cold Reg. Sci. Technol. 87 (2013) 47–58, https://doi.org/10.1016/j.coldregions.2012.12.003.
[5] R.B. Rutherford, R.L. Dudman, Aircraft De-Icing System, 2001. US Patent 6,330,986 B1.
[6] M.S. Park, Aircraft De-Icing System Using Thermal Conductive Fibers, Embry-Riddle Aeronautic University, Daytona Beach, FL, USA, 2015. M.Sc. Thesis.
[7] X. Huang, N. Tepylo, V. Pommier-Budinger, M. Budinger, E. Bonaccurso, P. Villedieu, L. Bennani, A survey of icephobic coatings and their potential use in a hybrid coating/active ice protection system for aerospace applications, Prog. Aerosp. Sci. 105 (2019) 74–97, https://doi.org/10.1016/j.paerosci.2019.01.002.
[8] W. Dong, M. Zheng, J. Zhu, G. Lei, Calculation and analysis of runback water flow on anti-icing airfoil surface, J. Aircr. 53 (2016) 1597–1605.
[9] X. Bu, G. Lin, J. Yu, S. Yang, X. Song, Numerical simulation of an airfoil electrothermal anti-icing system, Proc. Inst. Mech. Eng. Part G: J. Aerosp. Eng. 227 (2013) 1608–1622.
[10] D. De Pauw, A. Dolatabadi, Effect of superhydrophobic coating on the anti-icing and deicing of an airfoil, J. Aircr. 54 (2017) 490–499.
[11] E. Whalen, A. Broeren, M. Bragg, S. Lee, Characteristics of runback ice accretions on airfoils and their aerodynamics effects, in: 43rd AIAA Aerospace Sciences Meeting and Exhibit, 2005, January, p. 1065.
[12] F.J. Redondo, Innovative jet pump ice protection system for A400M, in: SAE 2015 International Conference on Icing of Aircraft, Engines, and Structures (No. 2015-01-2136), 2015, June.
[13] M. Soldado, Protección contra hielo en tomas de aire dinámicas de motores turbohélice, Universidad Politécnica de Madrid, 2021.
[14] Y. Shen, G. Wang, J. Tao, C. Zhu, S. Liu, M. Jin, Y. Xie, Z. Chen, Anti-icing performance of superhydrophobic texture surfaces depending on reference environments, Adv. Mater. Interfaces 4 (2017), 1700836.
[15] N. Abu Jarad, H. Imran, S.M. Imani, T.F. Didar, L. Soleymani, Fabrication of superamphiphobic surfaces via spray coating; a review, Adv. Mater. Technol. 7 (2022), 2101702.
[16] Y. Yuan, H. Xiang, G. Liu, L. Wang, H. Liu, R. Liao, Self-repairing performance of slippery liquid infused porous surfaces for durable anti-icing, Adv. Mater. Interfaces 9 (2022), 2101968.
[17] K. Alasvand Zarasvand, C. Pope, S. Nazari, D. Orchard, C. Clark, J. Brinkerhoff, K. Golovin, Durable metallic surfaces capable of passive and active de-icing, Adv. Eng. Mater. 24 (2022), 2200573.
[18] Y. Liu, Z. Zhao, Y. Shao, Y. Wang, B. Liu, Preparation of a superhydrophobic coating based on polysiloxane modified SiO2 and study on its anti-icing performance, Surf. Coat. Technol. 437 (2022), 128359.
[19] A. Dotan, H. Dodiuk, C. Laforte, S. Kenig, The relationship between water wetting and ice adhesion, J. Adhes. Sci. Technol. 23 (2012) 1907–1915, https://doi.org/10.1163/016942409X12510925843078.
[20] A. Lafuma, D. Quéré, Superhydrophobic states, Nat. Mater. 2 (2003) (2003) 457–460, https://doi.org/10.1038/nmat924.
[21] S. Alamri, V. Vercillo, A.I. Aguilar-Morales, F. Schell, M. Wetterwald, A.F. Lasagni, E. Bonaccurso, T. Kunze, Self-limited ice formation and efficient de-icing on superhydrophobic micro-structured airfoils through direct laser interference patterning, Adv. Mater. Interfaces 7 (2020), 2001231.
[22] V. Rico, J. Mora, P. García, A. Agüero, A. Borrás, A.R. González-Elipe, C. López-Santos, Robust anti-icing superhydrophobic aluminum alloy surfaces by grafting fluorocarbon molecular chains, Appl. Mater. Today 21 (2020), 100815.
[23] S. Jung, M. Dorrestijn, D. Raps, A. Das, C.M. Megaridis, D. Poulikakos, Are superhydrophobic surfaces best for icephobicity? Langmuir 27 (2011) 3059–3066.
[24] V. Hejazi, K. Sobolev, M. Nosonovsky, From superhydrophobicity to icephobicity: forces and interaction analysis, Sci. Rep. 3 (2013) 2194, https://doi.org/10.1038/srep02194.
[25] M. Nosonovsky, V. Hejazi, Why superhydrophobic surfaces are not always icephobic, ACS Nano 6 (2012) 8488–8491, https://doi.org/10.1021/nn302138r.
[26] S. Yang, Q. Xia, L. Zhu, J. Xue, Q. Wang, Q.M. Chen, Research on the icephobic properties of fluoropolymer-based materials, Appl. Surf. Sci. 257 (2011) 4956–4962, https://doi.org/10.1016/j.apsusc.2011.01.003.
[27] C. Peng, S. Xing, Z. Yuan, J. Xiao, C. Wang, J. Zeng, Preparation and anti-icing of superhydrophobic PVDF coating on a wind turbine blade, Appl. Surf. Sci. 259 (2012) 764–768, https://doi.org/10.1016/j.apsusc.2012.07.118.
[28] Y.L. Wu, W. She, D. Shi, T. Jiang, T.H. Hao, J. Liu, Q. Zang, J. You, R.Y. Li, An extremely chemical and mechanically durable siloxane bearing copolymer coating with self-crosslinkable and anti-icing properties, Compos. B. Eng. 195 (2020), 108031.
[29] B. Przybyszewski, A. Boczkowska, R. Kozera, J. Mora, P. Garcia, A. Aguero, A. Borras, Hydrophobic and icephobic behaviour of polyurethane-based nanocomposite coatings, Coatings 9 (2019) 811.
[30] T. Wong, S.H. Kang, S.K.Y. Tang, E.J. Smythe, B.D. Hatton, A. Grinthal, J. Aizenberg, Bioinspired self-repairing slippery surfaces with pressure-stable omniphobicity, Nature 477 (2011) 443–447, https://doi.org/10.1038/nature10447.
[31] P. Kim, T. Wong, J. Alvarenga, M.J. Kreder, W.E. Adorno-Martinez, Liquid-infused nanostructured surfaces with extreme anti-ice and anti-frost performance, ACS Nano 6 (2012) 6569–6577, https://doi.org/10.1021/Nn302310q.
[32] J. Chen, R. Dou, D. Cui, Q. Zhang, Y. Zhang, F. Xu, X. Zhou, J. Wang, Y. Song, L. Jiang, Robust prototypical anti-icing coatings with a self-lubricating liquid water layer between ice and substrate, ACS Appl. Mater. Interfaces 5 (2013) 4026–4030, https://doi.org/10.1021/am401004t.
[33] F. Veronesi, G. Boveri, J. Mora, A. Corozzi, M. Raimondo, Icephobic properties of anti-wetting coatings for aeronautical applications, Surf. Coat. Technol. 421 (2021), 127363, https://doi.org/10.1016/j.surfcoat.2021.127363.
[34] F. Wang, S. Xiao, Y. Zhuo, W. Ding, J. He, Z. Zhang, Liquid layer generators for excellent icephobicity at extremely low temperatures, Mater. Horiz. 6 (2019) 2063–2072, https://doi.org/10.1039/c9mh00859d.
[35] K. Golovin, A. Tuteja, A predictive framework for the design and fabrication of icephobic polymers, Sci. Adv. 3 (2017), e1701617, https://doi.org/10.1126/sciadv.1701617.
[36] C. Wang, T. Fuller, W. Zhang, K.J. Wynne, Thickness dependence of ice removal stress for a polydimethylsiloxane nanocomposite: sylgard 184, Langmuir 30 (2014) 12819–12826, https://doi.org/10.1021/la5030444.
[37] M. Shamshiri, R. Jafari, G. Momen, Potential use of smart coatings for icephobic applications: a review, Surf. Coat. Technol. 424 (2021), 127656.
[38] L. Wang, Q. Gong, S. Zhan, L. Jiang, Y. Zheng, Robust anti-icing performance of a flexible superhydrophobic surface, Adv. Mater. 28 (2016) 7729–7735, https://doi.org/10.1002/adma.201602480.
[39] P. Baumli, M. D'Acunzi, K.I. Hegner, A. Naga, W.S.Y. Wong, H.J. Butt, D. Vollmer, The challenge of lubricant-replenishment on lubricant-impregnated surfaces, Adv. Colloid Interf. Sci. 287 (2021), 102329, https://doi.org/10.1016/j.cis.2020.102329.
[40] J.M. Dubois, S.S. Kang, A. Perrot, Towards applications of quasicrystals, Mater. Sci. Eng. A 179 (1994) 122–126.
[41] E. Belin-Ferre, Quasicrystals: current topics, MRS Online Proc. Libr. Arch. 553 (1998) 347–358.
[42] J. Mora, P. García, R. Muelas, A. Agüero, Hard quasicrystalline coatings deposited by HVOF thermal spray to reduce ice accretion in aero-structures components, Coatings 10 (2020) 290.
[43] M. Mohseni, L. Recla, J. Mora, P.G. Gallego, A. Aguero, K. Golovin, Quasicrystalline coatings exhibit durable low interfacial toughness with ice, ACS Appl. Mater. Interfaces 13 (2021) 36517–36526.

[44] C. Laforte, Icephobic materials centrifuge adhesion test, in: Proceedings of the 11th International Workshop on Atmospheric Icing of Structures, IWAIS, Montreal, QC, Canada, 12–16 June 2005.
[45] A. Vicente, P.J. Rivero, P. García, J. Mora, F. Carreño, J.F. Palacio, R. Rodríguez, Icephobic and anticorrosion coatings deposited by electrospinning on aluminum alloys for aerospace applications, Polymers 13 (2021) 4164.
[46] A. Work, Y. Lian, A critical review of the measurement of ice adhesion to solid substrates, Prog. Aerosp. Sci. 98 (2018) 1–26.
[47] P.F. Ibáñez-Ibáñez, F.J. Montes Ruiz-Cabello, M.A. Cabrerizo-Vílchez, M. A. Rodríguez-Valverde, Mechanical durability of low ice adhesion polydimethylsiloxane surfaces, ACS Omega 7 (2022) 20741–20749.
[48] H. Niemelä-Anttonen, H. Koivuluoto, M. T°uominen, H. Teisala, P. Juuti, J. Harra, C. Stenroos, J. Lahti, J. Kuusipalo, J.M. Mäkelä, P. Vuoristo, J. Haapanen, Icephobicity of slippery liquid infused porous surfaces under multiple freeze–thaw and ice accretion–detachment cycles, Adv. Mater. Interfaces 5 (2018) 1–8, https://doi.org/10.1002/admi.201800828.
[49] Z. He, S. Xiao, H. Gao, J. He, Z. Zhang, Multiscale crack initiator promoted super-low ice adhesion surfaces, Soft Matter 13 (2017) 6562–6568.
[50] K. Golovin, S.P. Kobaku, D.H. Lee, E.T. DiLoreto, J.M. Mabry, A. Tuteja, Designing durable icephobic surfaces, Sci. Adv. 2 (2016), e1501496.
[51] E. Bonaccurso, M. Pervier, H. Pervier, E. Campazzi, G. Linassier, E. Goncalves, M. Balland, S. Suel, Deliverable 5.4. STORM-FP7-605180, 2017.
[52] H.H.G. Jellinek, Adhesive properties of ice, J. Colloid Sci. 14 (1959) 268–280.
[53] Y. Zhuo, S. Xiao, A. Amirfazli, J. He, Z. Zhang, Polysiloxane as icephobic materials–The past, present and the future, Chem. Eng. J. 405 (2021), 127088.
[54] J.K. Rader, B.G. Illston, Analysis of Anti-ice Coatings on Field Operational Anemometers, 2015.
[55] S. Xue, Y. Liu, Y. Wang, B. Xiao, X.X. Shi, J. Yao, X. Lv, W. Yuan, Y. He, Variation in anti-icing power of superhydrophobic electrothermal film under different temperatures and wind speeds, Int. J. Aerosp. Eng. (2022) 1–9.
[56] B. Hunt, C. Rawlins, B. Hill, An analysis of blade deicing techniques for multi-rotor UAV propellers, in: 2021 IEEE Aerospace Conference (50100), IEEE, 2021, March, pp. 1–6.
[57] C. Antonini, A. Amirfazli, M. Marengo, Superhydrophobicity or icephobicity for an effective icing mitigation strategy?, in: International Heat Transfer Conference Digital Library Begel House Inc, 2014.
[58] Y. Shen, X. Xie, J. Tao, H. Chen, Z. Cai, S. Liu, J. Jiang, Mechanical equilibrium dynamics controlling wetting state transition at low-temperature superhydrophobic Array-microstructure surfaces, Coatings 11 (2021) 522, https://doi.org/10.3390/coatings11050522.
[59] L. Wang, Z. Tian, G. Jiang, X. Luo, C. Chen, X. Hu, H. Zhang, M. Zhong, Spontaneous dewetting transitions of droplets during icing & melting cycle, Nat. Commun. 13 (2022) 1–15.
[60] Y. Yan, Z. Jia, Y. Yang, Preparation and mechanical properties of PTFE/nano-EG composites reinforced with nanoparticles, Procedia Environ. Sci. 10 (2011) 929–935.
[61] P.F.Ibáñez Ibáñez, Design and Preparation of Icephobic Metal-based Surfaces, 2021.
[62] Z. Zhao, H. Chen, X. Liu, Z. Wang, Y. Zhu, Y. Zhou, Novel sandwich structural electric heating coating for anti-icing/de-icing on complex surfaces, Surf. Coat. Technol. 404 (2020), 126489.
[63] Z. Zhao, H. Chen, X. Liu, H. Liu, D. Zhang, Development of high-efficient synthetic electric heating coating for anti-icing/de-icing, Surf. Coat. Technol. 349 (2018) 340–346.
[64] J. Hu, G. Jiang, Superhydrophobic coatings on iodine doped substrate with photothermal deicing and passive anti-icing properties, Surf. Coat. Technol. 402 (2020), 126342.
[65] X. Liu, H. Chen, Z. Zhao, Y. Yan, D. Zhang, Slippery liquid-infused porous electric heating coating for anti-icing and de-icing applications, Surf. Coat. Technol. 374 (2019) 889–896.